Title

On-Surface Polyarylene Synthesis by Cycloaromatization of Isopropyl Substituents

Author list

Amogh Kinikar°[1], Marco Di Giovannantonio°[1,5], José I. Urgel[1,6], Kristjan Eimre[1], Zijie Qiu[2], Yanwei Gu[2], Enquan Jin[2], Akimitsu Narita[2,7], Xiao-Ye Wang[2,8], Klaus Müllen*[2,3], Pascal Ruffieux[1], Carlo Pignedoli*[1], and Roman Fasel*[1,4]

° These authors contributed equally

* Address correspondence to these authors

Affiliations

[1]Empa, Swiss Federal Laboratories for Materials Science and Technology, 8600 Dübendorf (Switzerland)

[2]Max Planck Institute for Polymer Research, 55128 Mainz (Germany)

[3]Institute of Physical Chemistry, Johannes Gutenberg - Universität Mainz, 55128 Mainz (Germany)

[4]Department of Chemistry, Biochemistry and Pharmaceutical Sciences, University of Bern, 3012 Bern (Switzerland)

Current address:

[5]Istituto di Struttura della Materia-CNR (ISM-CNR), via Fosso del Cavaliere 100, Roma 00133 (Italy)

[6]IMDEA Nanoscience, C/Faraday 9, Campus de Cantoblanco, Madrid 28049 (Spain)

[7]Organic and Carbon Nanomaterials Unit, Okinawa Institute of Science and Technology Graduate University, 1919-1 Tancha, Onna-son, Kunigami-gun, Okinawa, 904-0495 (Japan)

[8]State Key Laboratory of Elemento-Organic Chemistry, College of Chemistry, Nankai University, Tianjin 300071 (China)

Email addresses:

Klaus Müllen: muellen@mpip-mainz.mpg.de

Carlo Pignedoli: carlo.pignedoli@empa.ch

Roman Fasel: roman.fasel@empa.ch

Abstract

Immobilization of organic molecules on metal surfaces and their coupling via thermally induced C-C bond formation is an important technique in organic and polymer synthesis. Using this approach, insoluble and reactive carbon nanostructures can be synthesized and the reactions monitored *in situ* using scanning probe methods. The diversity of conceivable products, however, is limited by the number and variety of known on-surface reactions. Here, we introduce the on-surface synthesis of polyarylenes by intermolecular oxidative coupling of isopropyl substituents of arenes. This [3+3] dimerization reaction forms a new phenylene ring and can be regarded as a formal cycloaromatization. The synthetic value of this reaction is proven by the synthesis of polyarylenes and co-polyarylenes, which we demonstrate by synthesizing poly(2,7-pyrenylene-1,4-phenylene). Scanning tunnelling microscopy and non-contact atomic force microscopy studies complemented by density functional theory calculations offer mechanistic insights into the on-surface cycloaromatization reaction.

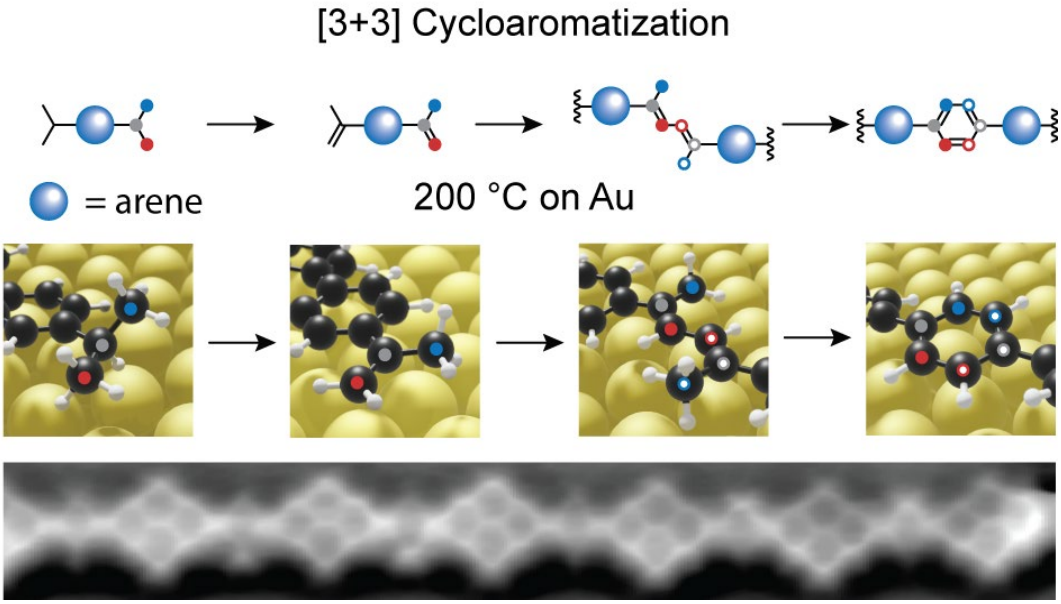

Main text

Introduction

The synthesis of new conjugated polymers with specific properties depends critically on the choice of the building blocks and the mode of repetitive bond formation[1,2]. When targeting optical and charge-transport properties, polyarylenes are playing a key role as functional materials[3,4]. This is because polyarylenes can comprise not only phenylene repeat units, but also their heterocyclic analogs or higher polycyclic aromatic hydrocarbons, allowing for the careful tuning of their electronic properties[5,6]. The Suzuki reaction, which allows for the strictly alternating incorporation of different arylenes, has thus far met the urgent needs of materials science[5]. In particular, donor-acceptor (co-)polymers consisting of alternating arrays of electron-rich and electron-deficient moieties have played an important role as semiconductors in organic field-effect transistors with high charge-carrier mobilities[7–10]. More recently, the need for toxic organometallic compounds and expensive boronic ester precursors have been circumvented by direct (hetero)arylation polymerization[11–13] and oxidative C-H/C-H arylation polymerization[14], which, however, raises issues of regioselectivity.

Recently, a new protocol of polymer synthesis has become available by depositing dihaloarenes on metal surfaces and the subsequent activation of these monomers by thermal carbon-halogen cleavage, followed by polymerization of the intermediate diradicals[15] (Fig. 1a). In the so-called on-surface Ullman-type coupling, the metal surface acts as a catalyst, and so a crucial difference from the Ullmann coupling in solution should be noted: the conventional solution process comprises an electron transfer and the halogen is removed as halide anion, whereas the on-surface reaction proceeds via a homolytic carbon-halogen bond cleavage leading to surface-stabilized carbon radicals. Such radicals undergo homo-coupling, and non-stochastic alternating copolymerization of different building blocks is not feasible under these conditions. We are thus limited to the incorporation of, for example, two phenylene as linkers between arenes, but never a single phenylene ring. However, on-surface synthesis offers two fascinating advantages[16–18]: i) unstable products, which would not survive in solution, can become available due to the ultra-high vacuum conditions and stabilization by the metal surface[19–21], and ii) the reaction intermediates and products can be characterized *in situ* by scanning probe microscopy thus providing key mechanistic information on the reaction pathway[22,23].

Are there other reactions possible for on-surface polymer synthesis? In general, reactions that can convert aliphatic to aromatic hydrocarbons are desirable since aliphatic hydrocarbons are available in abundance. The immobilization of suitable precursors on metal surfaces can intrinsically activate specific C-H bonds that are closer to the catalytic metal substrate, such as the terminal C-H bonds on linear alkanes[24], activation of which in solution would require specific directing groups. A related case of cycloaromatization in solution is the Pd(II)-induced oxidative coupling of *α*-olefins to tetra-substituted butadienes, whereby prolonged oxidation can also lead to benzene formation by cycloaromatization[25]. However, more generally in solution chemistry cycloaromatization reactions depend on reactive hydrocarbons such as diynes, which are known to undergo Bergman cyclization through a diradical intermediate to form aromatic rings[26]. Thereby, the diradical must be quenched by the addition of a hydrogen

source such as 1,4-cyclohexadiene to avoid uncontrolled polymerization. Interestingly, the same reaction, when performed on a metal surface, but without a quencher, opens up a way toward polymers[27]. Direct and well-defined cycloaromatization of alkanes, however, has not yet been achieved.

Herein, we describe an intriguing on-surface reaction, namely the selective formation of phenylene rings by a formal [3+3] cycloaromatization of two isopropyl-substituted arylenes on Au(111) and Au(110) surfaces (Fig. 1b). This cycloaromatization is unprecedented as it starts from relatively unreactive alkyl groups rather than from reactive allyl or diyne species. We characterize the chemical structure of the products and the stable reaction intermediates by scanning tunneling microscopy (STM) and non-contact atomic force microscopy (nc-AFM). These experimental results are supported by density functional theory (DFT) calculations, which help to identify the reaction intermediates and provide activation barriers for each reaction step, thus creating a complete mechanistic picture of the cycloaromatization.

Results and Discussion

Polymerization via [3+3] cycloaromatization on Au surfaces

The reaction illustrated in Fig. 1b furnishes a new phenylene ring by a formal [3+3] cycloaromatization of two isopropyl substituents. To explore this unprecedented on-surface reaction, diisopropyl-*p*-terphenyl **1** was synthesized (see the Supplementary Information Section 1) as a model compound for the following reasons: i) the presence of the two isopropyl substituents should allow for the formation of polymers by surface-assisted cycloaromatization, ii) *p*-terphenyl has already been well-studied on Au surfaces, and, due to its suitable molecular size, can be deposited under UHV conditions, iii) crucially, the newly formed phenylene rings can be identified by comparison with the existing ones as reference.

As will be demonstrated below, the isopropyl cycloaromatization reaction takes place via two stable intermediates **2** and **3** (Fig. 2a). The reaction is initiated by Au-catalyzed selective dehydrogenation of the isopropyl toward isopropenyl groups in **2**. This follows from the specific adsorption geometry of **1** on the Au surface that breaks the equivalence of the methyl groups (Fig. 2b). Polymerization then proceeds by intermolecular C-C coupling between the methylene carbons (CH_2) (labeled red) leading to the formation of **3** (see Fig. 2c-d). Polymer **3** then undergoes cycloaromatization to form the new phenylene ring leading to **4** (see Fig. 2d-e).

To investigate the polymerization process, **1** is deposited on a clean Au(111) surface held at 200 °C under ultrahigh vacuum (UHV) conditions. For STM imaging, the surface is then cooled down to 4.5 K. STM images such as the one shown in Fig. 2f reveal the formation of linear chains (several being ~10 nm in length), demonstrating that polymerization has occurred (the length of monomer **1** is 1.8 nm) (see Fig. 2f). The longer chains appear uniform along their polymerization direction, suggesting that the resulting structure is periodic. However, the chains are frequently cross-linked, as the Au(111) surface is isotropic with a threefold symmetry and therefore allows polymerization along different directions [28]. The cross-linking can be completely avoided, however, by performing the reaction on the anisotropic Au(110) surface, where the missing row reconstruction induces a one-dimensional (1D) constraint on the diffusion of the molecules so that they favor motion along the rows of the reconstructed surface[24]. When **1** is deposited on the Au(110) surface and annealed at 200 °C, very long polymer chains without any cross-linking are found, some of which are longer than 80 nm (see Fig. 2g, h). Therefore, the synthesis of extended chains on Au(111) and Au(110) leaves no doubt that polymerization occurs by the activation of the isopropyl groups.

Experimental identification of the reaction intermediates

The progress of the reaction can be monitored by depositing **1** on Au(111) held at room temperature, followed by annealing to successively higher temperatures, and recording STM images of the surface at each step (Supplementary Fig. S1). STM images obtained after depositing the molecule at room temperature exhibit bulky protrusions at the ends of the molecule due to the presence of the non-planar isopropyl group in **1** (Supplementary Fig. S1). Upon annealing to 180 °C, these protrusions start to disappear and the molecules appear entirely planar, as is expected for the isopropenyl species **2**. While some molecules have already undergone C-C coupling at 180 °C, extensive coupling is observed after annealing to 200 °C. When two isopropenyl groups homo-couple at their CH_2 sites to form **3,** they appear as jointed connections, while upon cycloaromatization the newly formed phenylene units in **4** lead to smooth junctions and determine the end-point of the reaction, as the phenylene ring formed is no longer reactive at 200 °C on Au surfaces[28].

To unequivocally establish the chemical identities of **1**-**4** we perform nc-AFM imaging of samples obtained by successive annealing steps. nc-AFM acquired with a CO-functionalized tip leads to an enhanced interaction with the adsorbates on the surface and allows for the resolution of individual molecular bonds and thus a rather straightforward determination of chemical structure[29,30]. In the following, we discuss STM (Fig. 3b-e) and nc-AFM images (Fig. 3f-i) obtained after deposition of **1** on Au(111) at room temperature, after annealing at 180 °C, and after annealing at 200 °C to unravel the chemical structures (Fig. 3a) of **1**, **2**, and, **3** and **4**, respectively. We compare the experimental results with Probe-Particle model simulations[31] (Fig. 3j-m) on the DFT-optimized structures (top view: Fig. 3n-q and side view: Fig. 3r-u) .

In Fig. 3f, acquired after room temperature deposition of **1**, the bulky isopropyl groups appear as bright protrusions at the ends of the molecule. This is due to the protrusion of the methyl groups above the plane of the terphenyl backbone (Fig. 3r), which prevents a closer tip approach. The terphenyl backbone is thus not clearly resolved. Similar bright protrusions are obtained in nc-AFM image simulations (Fig. 3j) using the probe particle model for the optimized geometry of **1** on Au(111)[31]. After the first dehydrogenation step of **1**, which occurs upon annealing to 180 °C, the resulting isopropenyl group in **2** (Fig. 3 g,k) has a much more planar adsorption geometry as can be seen in Fig. 3s. Species **2** can hence be imaged with a lower tip height, thus resolving the atomic bonds, and provides direct confirmation of the identity of **2.**

The chemical structure of the intermolecular coupling motif is revealed in nc-AFM images of **3** obtained after annealing to 200 °C (Fig. 3d). The coupling is found to occur at the methylene carbon of the isopropenyl group, as the nc-AFM images show the bright protrusions of the methyl carbons are adjacent to the site at which polymerization has occurred. Moreover, the termini of the chain still exhibit the same features as the ends of **2**, providing evidence that they are still "active" and can undergo further polymerization. The simulated nc-AFM image of the optimized structure of **3** (Fig. 3l), together with the corresponding DFT-optimized geometry depicted in Fig. 3p,t, are in remarkably good agreement with the experimental result (See Supplementary Fig. S3 for a discussion of the twist angle of the phenylene rings). However, to further confirm the identity of the junction, similar nc-AFM simulations of optimized geometries of other plausible junctions are compared with the experimental data, and agreement is only

found with the 2,4-hexadiene junction (Supplementary Fig. S4). This confirms the assigned structure of **3** and the proposed coupling motif.

Finally, cycloaromatization leads to the formation of a new phenylene ring in **4**. We confirm this by scanning an extended chain with four precursor units (Fig. 3i). The newly formed six-membered rings (highlighted with white arrows in Fig. 3i) appear completely identical to the ones of the terphenyl moieties. Their appearance is also in excellent agreement with the simulated nc-AFM image (Fig. 3m) of the optimized structure (Fig. 3q,u), which conclusively shows that the cycloaromatization product is a phenylene ring.

The first step of this reaction sequence is the selective dehydrogenation of **1** to form **2**. Since **2** is a stable compound, it can be synthesized *ex-situ* and deposited on Au(111) for the sake of comparison, providing further confirmation of the relevant first step of the proposed reaction pathway. The nc-AFM image of the as-synthesized 4,4''-di-prop-2-enyl-*p*-terphenyl (DPTP) deposited on Au(111) (Supplementary Fig. S5c-d) is identical with that obtained for **2** occurring as an intermediate, and subsequent annealing of DPTP furnishes similar polymer chains as those achieved from **1** (Supplementary Fig. S5e), establishing the selective dehydrogenation of the isopropyl group to isopropenyl as the first step of the reaction sequence.

Reaction mechanism investigated by *ab initio* calculations

For surface-catalyzed reactions, the DFT level of theory has recently proven to reliably capture molecule-molecule and molecule-substrate interactions in order to access the relevant energy barriers[32]. To characterize the reaction path for the [3+3] cycloaromatization we have simulated both the substrate and the adsorbates at the DFT level of theory and performed constrained geometry optimizations along specific reaction coordinates (see Methods and Supplementary Fig. S6 for the special case of **3b** to **3c**). The results of the reaction path calculations are summarized in Fig. 4Fig. 4. The first step of the reaction pathway is the selective dehydrogenation of the isopropyl group of **1** to the isopropenyl group of **2**. It begins with the cleavage of the C-H bond at the tertiary carbon atom (labeled with a grey dot in Fig. 4) with an energy barrier of $E_{1\,1a}$ =1.6 eV. The barrier for removal of a hydrogen atom first from the $–CH_3$ carbon in **1** would be much higher (2.8 eV, Supplementary Fig. S6), which is thus highly disfavored at the reaction temperature of ~200 °C. However, cleavage of the C-H bond at the $–CH_3$ carbon (red) atom *after* the formation of the tertiary radical has a much smaller barrier of $E_{1a\,2}$ =0.7 eV, and results in the formation of the isopropenyl group in **2**. This reduction is largely due to the formation of a bond between the carbon radical (grey dot) and the underlying surface, which brings the terminal methyl groups closer to the catalytically active surface, thus lowering the dehydrogenation barrier[33,34]. The effective barrier for the selective dehydrogenation step from **1** to **2** is thus found to be 1.6 eV.

Intermolecular coupling of **2** could either occur through cleavage of the C-H bond at the sp^2 carbon (highlighted by a red dot) or by direct C-C bond formation (without dehydrogenation) leading to the formation of a diradical intermediate **2a**. We find that the energy barrier for C-H bond cleavage from the red carbon atom is 2.2 eV (Supplementary Fig. S6c) while the energy barrier for direct C-C coupling to the diradical intermediate **2a** is only $E_{2\,2a}$ =1.2 eV. A diradical pathway is thus strongly favored. Such a mechanism is not unexpected and has similarities to the Flory mechanism proposed for the self-initiation of styrene polymerization[35]. Although the energy barrier for this coupling step is only 1.2 eV, it relies on

the encounter of two molecules in their proper conformations which likely results in a low attempt frequency, thus slowing down this step of the reaction.

The final step is the cycloaromatization of the hexadiene bridge in **3**, which starts with the sequential cleavage of a C-H bond from the two CH_3 groups, with energy barriers of 1.6 eV and 1.4 eV. After cyclization, the newly formed six-membered ring is then aromatized by a sequential loss of hydrogens, completing the cycloaromatization process to form **4**. The effective barrier for the complete cycloaromatization step from **3** to **4** is determined by the **3b** to **3d** transition and is 1.6 eV. It is comparable to the effective barrier for the formation of **2** from **1**. Indeed, species **2**, **3**, and **4** are observed simultaneously, suggesting comparable effective energy barriers for their formation. The temperature range of the reaction (~200 °C) corresponds to an activation energy of 1.4 eV, which is in reasonable agreement with 1.6 eV, the value obtained by these calculations (Supplementary Fig. S7).

We note that the energies shown in Fig. 4 consider the cleaved hydrogens to have desorbed from the surface by the formation of H_2, which results in an energy gain of -1 eV per hydrogen atom[36]. Moreover, each step in which hydrogen is lost (indicated by -H on the energy profile) from the surface is irreversible. The cumulative energy gain for the Au surface-catalyzed [3+3] cycloaromatization is thus -5.7 eV, rendering this a strongly exothermic reaction (see Supplementary Fig. S6 for an energy profile neglecting the desorption of H_2).

Scope and limitations of the reaction

We demonstrate the potential of this new phenylene-ring forming reaction by synthesizing a copolymer (a polyarylene with two different arylene groups) with strictly alternating arylene and phenylene moieties. The prototypical copoly(arylenephenylene) is obtained by depositing 2,7-diisopropylpyrene (**5**) (Fig. 5a) onto the Au(111) surface held at 235 °C. STM images of the surface after deposition of **5** show that the molecule has polymerized into linear chains of poly(2,7-pyrenylene-1,4-phenylene) **7** (Fig. 5b). Bond-resolved nc-AFM images of a segment of the polymer clearly reveal the chemical structure of the expected copolymer with alternating pyrenylene and phenylene moieties and nc-AFM simulations of a tetrameric chain are in excellent agreement with experimental results (Supplementary Fig. S9), confirming the synthesis of **7**. Additionally, nc-AFM images of non-polymerized precursor molecules (Supplementary Fig. S8) point toward the existence of **6** where the isopropyl groups have dehydrogenated to isopropenyl groups as expected.

We have also acquired bond-resolved nc-AFM images to understand the occurrence of cross-links (Supplementary Fig. S10). Since pyrene is expected to remain intact at 235 °C on Au(111), the carbon atoms constituting the newly formed aromatic rings at the cross-links must stem from the isopropyl group. We observe a variety of different ring geometries at the cross-links, some of which are only possible by rearrangement of the carbon atoms from the isopropyl group. Such changes are most likely to occur during the cycloaromatization step and are thought to be the result of a reaction between the reactive radical intermediates (e.g. **3a-b** in Fig. 4) [23,37]. The cross-links are thus the result of cycloaromatization of an extended aliphatic carbon chain and provide preliminary evidence that the cycloaromatization process described here for the hexadiene link may be extended to longer carbon chains. In addition, as with **1**, the degree of cross-linking can be greatly reduced by performing the on-surface synthesis on an Au(110) substrate. Under these conditions, **5** polymerizes to uniaxially aligned **7** with no cross-linking

(Supplementary Fig. S11). The uniaxially oriented growth of these polymers makes them a prime candidate for transfer to technologically relevant substrates using established methods[38,39].

It may seem trivial, but as has been already mentioned, an indispensable prerequisite for cycloaromatization is that the isopropyl-substituted arenes remain adsorbed on the Au surface at the reaction temperature of ~200 °C. This places a limit on the use of low molecular weight precursor molecules, since their surface interaction is weak. For instance, annealing 9,10-diisopropenylanthracene **8** (Fig. 6a) on an Au(111) surface to the reaction temperature of 200 °C failed to give detectable products as the molecule desorbed before polymerization could occur (Supplementary Fig. S12).

The reactivity of the radical intermediates can lead to cross-linking, but it could also undergo the formation of new intra-molecular rings. We have investigated 10-isopropenyl-10'-isopropyl-9,9'-bianthracenyl (**9**) (Fig. 6b), which was originally designed to obtain a perianthracene-phenylene copolymer through the planarization of the bianthracenyl unit and the [3 + 3] cycloaddition of the isopropyl/isopropenyl substituents upon activation on the Au(111) surface at ~ 200 °C (Supplementary Fig. S13). Strikingly, we observe instead the formation of polymers with five-membered rings that are mirror-symmetric across the planarized perianthracene core (surface assisted cyclodehydrogenation can occur at 200 °C[40]) namely with the dicyclopenta[*cd*,*lm*]perylene substructure (Fig. 6c), as shown in the bond-resolved STM image of **10** acquired with a CO-functionalized tip recorded in the Pauli repulsion regime[41,42] (Fig. 6d).This clearly shows that while inter-molecular coupling can occur, the formation of the phenylene rings is suppressed when the isopropyl group is installed on a zigzag edge and the formation of intramolecular five-membered rings is preferred instead. Efforts to understand the mechanism behind the selective formation of polymer **10** with five-membered rings are ongoing.

Conclusions

The past decade has brought remarkable synergies of chemistry, materials science, and nanoscience. Polyarylene synthesis, either in solution or on surfaces, meets major needs of research into conjugated polymers, even more so since more complex topologies such as macrocycles or highly branched homologs have become available. The further development of the field requires new synthesis concepts. The transformation of alkyl and alkenyl precursors into aromatic products is of special value since these are amply available from natural sources. Selective activation of C-H bonds is, thereby, mandatory which in turn requires a deeper understanding of the underlying catalytic mechanisms. Here we have reported the Au surface-catalyzed [3+3] cycloaromatization of isopropyl substituents on arenes to form phenylene rings. Combining nc-AFM for structure identification and DFT-based calculations for reaction barriers has achieved the comprehensive elucidation of the reaction mechanism. We have also demonstrated the use of this reaction in the synthesis of copolymers. Isopropyl substitution on arenes thus provides an easy on-surface pathway for their polymerization with phenylene linkers and adds an important, fully characterized reaction to the on-surface synthesis toolbox. Finally, the ability to grow these polymers in a uniaxially oriented manner and their transfer to technologically relevant substrates makes this on-surface route to copolymers potentially very appealing as desired properties can be achieved by designing the right isopropyl substituted arene precursors.

Methods

STM and nc-AFM experiments

The on-surface synthesis experiments were carried out under ultrahigh vacuum conditions with a base pressure of 2×10^{-10} mbar. The Au substrates (MaTeck GmbH) were cleaned by repeated cycles of Ar^+ ion sputtering (1 keV) and subsequent annealing (400 °C < T < 450 °C). All the molecules were sublimated onto the cleaned surfaces *in situ* from quartz crucibles using a custom-made evaporator. The sublimation rate of the molecules was determined using a quartz crystal microbalance and the sublimation temperature was adjusted to get the required rate. For room temperature deposition a sublimation rate of 2 monolayers per hour was used while for deposition on a hot surface a much slower rate of 0.01 monolayer per hour was used. Slow deposition on a hot surface was used to reduce cross-linking by achieving pseudo high-dilution[43], where the reaction intermediates after coupling of two molecules (such as **3b**) can complete the reaction before encountering a third molecule. The surface temperature was measured by a pyrometer (Optris) for surface temperatures above 150°C and a thermocouple contact on the sample plate for lower temperatures. STM and nc-AFM images were acquired with a low-temperature scanning tunneling microscope (Scienta Omicron) operated at 4.7 K with a tungsten tip placed on a qPlus tuning fork sensor[44]. The tip was functionalized with a single CO molecule at the tip apex picked up from the previously CO-dosed surface[45]. The sensor was driven at its resonance frequency (27500 Hz) with a constant amplitude of 70 pm. The frequency shift from the resonance of the tuning fork was recorded in constant-height mode using Omicron Matrix electronics and HF2Li PLL by Zurich Instruments. The Δz is positive (negative) when the tip-surface distance is increased (decreased) with respect to the STM set point at which the feedback loop is open. Δz is set to zero when the feedback loop is switched off.

Computational details

All DFT calculations were performed with the AiiDAlab platform[46] based on AiiDA[47] and the CP2K code[48]. The surface-adsorbate systems were modeled within the repeated slab scheme. The simulation cell consisted of 4 atomic layers of Au along the [111] direction. A layer of hydrogen atoms was used to passivate one side of the slab to suppress the Au(111) surface state. 40 Å of vacuum was included in the simulation cell to decouple the system from its periodic replicas in the direction perpendicular to the surface. The electronic states were expanded with a TZV2P Gaussian basis set[49] for C and H species and a DZVP basis set for Au species. A cutoff of 600 Ry was used for the plane-wave basis set. Norm-conserving Goedecker-Teter-Hutter pseudopotentials[50] were used to represent the frozen core electrons of the atoms. We used the PBE parameterization for the generalized gradient approximation of the exchange-correlation functional.[51] To account for van der Waals interactions, we used the D3 scheme proposed by Grimme.[52] The gold surface was modeled using a supercell, with its size ranging from 39.8×40.0 Å^2 (corresponding to 896 Au atoms) to 81.0×24.7 Å^2 (1120 Au atoms) depending on the dimensions of the adsorbate. The Au(111) slab was planar, and the herringbone reconstruction

associated with this surface was not considered as it would greatly expand the supercell and not significantly change the chemical activity of the surface[53]. To obtain the equilibrium geometries, we kept the atomic positions of the bottom two layers of the slab fixed to the ideal bulk positions, and all other atoms were relaxed until forces were lower than 0.005 eV/Å. For nc-AFM simulations with AiiDAlab, the equilibrium geometries and the electrostatic potential obtained with CP2K are used in combination with the probe particle code developed by Hapala[54].

For the characterization of the reaction path of the cycloaromatization reaction, using advanced sampling methods such as meta-dynamics[55] would be computationally prohibitive due to the large number of atoms involved. Also relying on the Nudged Elastic Band[56] or String Method[57] for such a long series of reaction steps would have a computational cost that we cannot afford. In order to nevertheless obtain a reasonable estimate of the reaction barriers, we use constrained geometry optimizations by defining a collective variable (length of a bond between two atoms or amplitude of a dihedral angle) for each step of the reaction pathway based on the chemical identity of the intermediates identified in Fig. 3. This collective variable is varied with a fine step size to sample the potential energy with adequate accuracy. Each intermediate geometry is optimized without constraints. The energy profile resulting from such a series of constrained geometry optimizations, where all atomic degrees of freedom are allowed to relax subject to the constraint of the collective variable, provides a reasonable estimate of the reaction barrier. In the reaction step from **3b** to **3c**, however, a single collective variable did not provide a satisfactory description of the reaction path, and we resorted to a NEB calculation for this step. The NEB calculations were performed on 24 replicas interpolating **3b** to **3c** with inter-replica distances less than 1.4 Å.

Data Availability

All the STM, nc-AFM and computational datasets shown in the manuscript and the supporting information are available from: doi.org/10.24435/materialscloud:yy-sc[58]

Code Availability

The CP2K software package is available at: https://www.cp2k.org/ and AiiDAlab software package can be downloaded at: https://www.materialscloud.org/work/aiidalab.

Acknowledgements

This work was supported by the Swiss National Science Foundation (Grant No. 200020_182015), the NCCR MARVEL funded by the Swiss National Science Foundation (Grant No. 51NF40-182892), the Johannes Gutenberg-Universität Mainz (JGU) through Gutenberg Forschungskolleg Fellowship (GFK) and the Max Planck Society. J.I.U. acknowledges the European Union's Horizon 2020 research and innovation programme under the Marie Skłodowska-Curie (Grant agreement No. 886314). E.J., Y.G. and Z.Q would like to acknowledge support from the Alexander von Humboldt Foundation. K.M. thanks the Gutenberg Research College for a scholarship. Computational support from the Swiss Supercomputing Center (CSCS) under project ID s904 is gratefully acknowledged. A.K., M.D.G., J.I.U., P.R. and R.F. thank Lukas Rotach (Empa, Dübendorf) for technical support.

Author Contributions Statement

A.K., K.M., P.R., and R.F. conceived the project. Z.Q., Y.G., E.J., and X.-Y.W. synthesized and characterized the precursor molecules under the supervision of A.N. and K.M.. A.K., M.D.G., and J.I.U. performed the on-surface synthesis and the STM / nc-AFM measurements under the supervision of P.R. and R.F.. K.E. made the DFT nc-AFM simulations, C.A.P. did the DFT constrained geometry replica chain and NEB calculations. A.K. and K.M. wrote the manuscript with input from all authors.

Competing Interests Statement

The authors declare no competing interests.

Figure Legends/Captions

a Ullmann-type coupling reaction of arene substituents

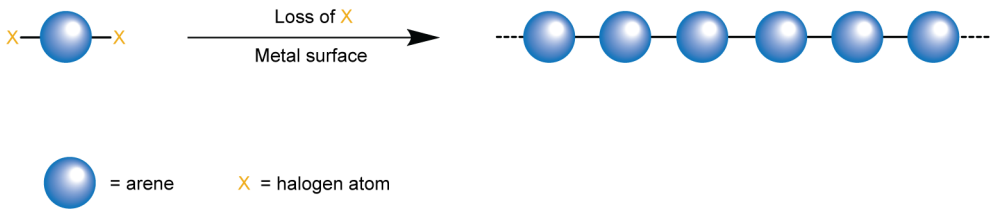

b This work: formal [3+3] cycloaromatization of isopropyl substituents

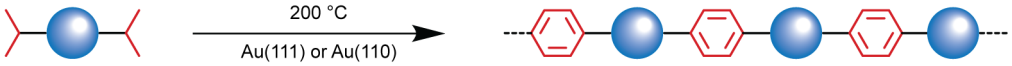

Fig. 1 | On-surface polyarylene synthesis. a, direct ring coupling of a dihalo-arene[15], **b**, coupling of two isopropyl substituted arylenes resulting in a repetitive [3+3] cycloaromatization process.

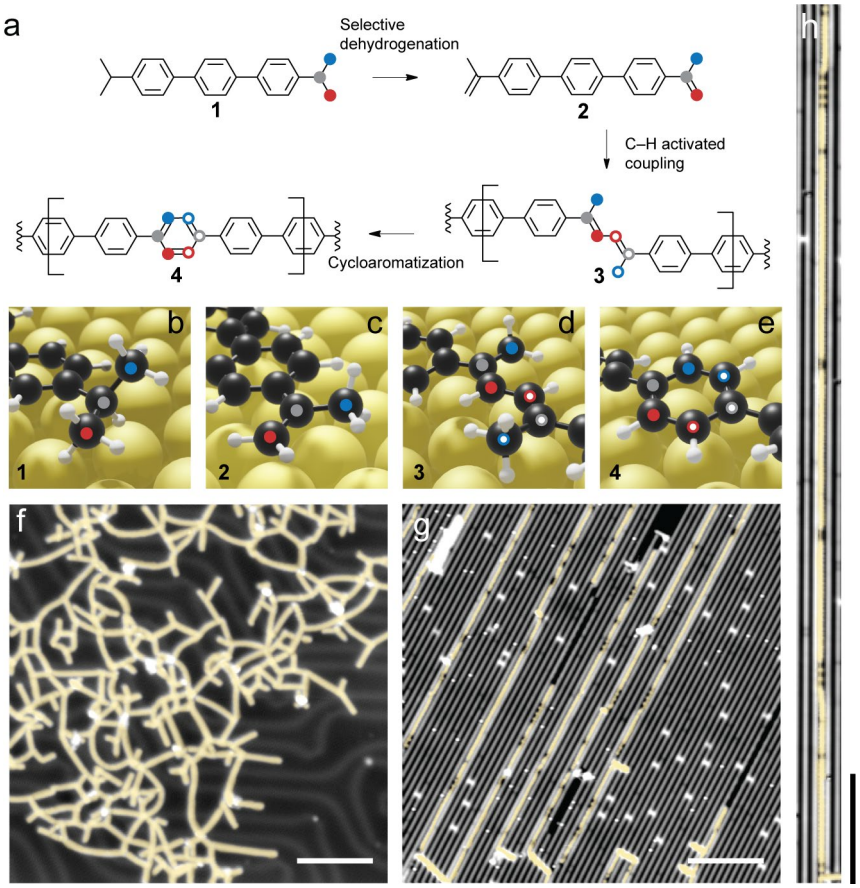

Fig. 2 | Formation of new phenylene rings by the homocoupling of diisopropyl-substituted terphenyl on Au(111) and Au(110) surfaces. a, The summarized pathway from **1** to **4** through the [3 + 3] cycloaromatization of a pair of isopropyl substituents to form a phenylene ring. In **a-e**, the carbon atoms involved in the reaction sequence are labeled with red, blue, and grey circles. The first step is the dehydrogenation of the isopropyl group of **1** to yield the propenyl group in **2** (marked by double bond formation between the red and the grey carbon atoms). Subsequently, the intermediate **2** couples at the site of the carbon atoms marked in red (hollow circles are used to indicate the second monomer for the formation of the polymer) to give **3**. In the last step, the alkenyl link of **3** undergoes cycloaromatization producing the new phenylene rings of **4**. As there are two reaction sites in **1**, the homocoupling can occur at both ends, leading to the formation of polymers. **b-e**, DFT optimized structure of the reaction sites in **1**, **2**, **3,** and **4** respectively. **f**, STM image acquired after deposition of **1** on Au(111) held at 200 °C, where cross-linked linear polymer chains are found (tunneling conditions: V = -1 V, I = 100 pA). **g**, Formation of long polymers on Au(110) by deposition of **1** and subsequent annealing at 200 °C. The polymers are aligned along the missing row reconstruction of the Au(110) surface (V = -0.5 V, I = 50 pA). **h**, An example of a polymer longer than 80 nm. The change in contrast along the length of the polymer is due to a change in the adsorption geometry of the polymer chain[59] (V = 0.02 V, I = 100 pA). To better distinguish the linear polymers from the linear reconstruction of the Au(110) surface, all polymers in **f-h** (all scale bars are 10 nm) have been tinted yellow.

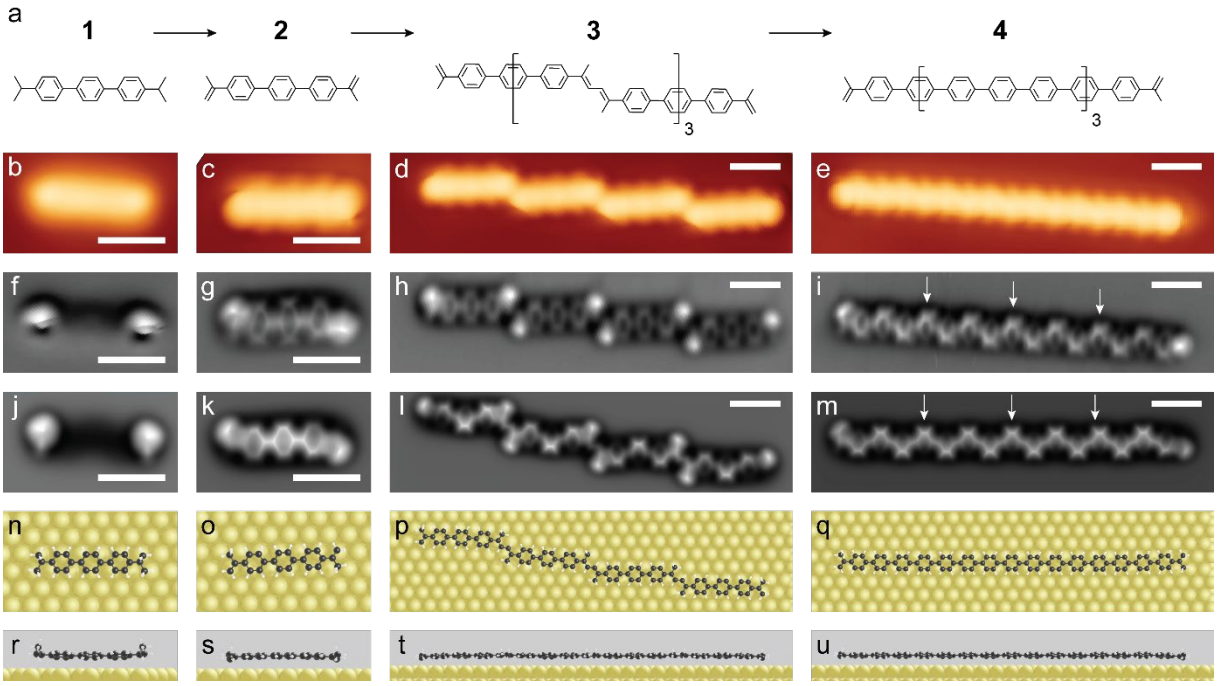

Fig. 3 | Confirmation of chemical structures of 1 to 4. Experimental STM and high-resolution nc-AFM images, together with simulated nc-AFM images and DFT optimized geometries of **1**, **2**, **3**, and **4** on Au(111) for proof of the chemical structures. The bulky isopropyl group prevents the resolution of the terphenyl backbone upon nc-AFM visualization of **1**. Upon planarization to isopropenyl groups in **2**, however, the three phenylene units can be clearly resolved. The ends of the molecule have a single bright protrusion due to the CH_3 group while the CH_2 group appears less bright as it is at the same height as the phenylene repeat units. Images obtained on **3** reveal bright protrusions that are characteristic of the CH_3 group adjacent to the newly formed C-C bond, proving that polymerization occurs by intermolecular C-C coupling at the CH_2 sites. A linear chain of 15-phenylene rings in **4** results from cycloaromatization of four precursor moieties. The newly formed rings, highlighted by white arrows, are identical to those already present in the terphenyl backbone, thus confirming their identity as phenylene rings. **a**, Chemical structure of **1**, **2**, **3**, and **4**, and the process of the reaction. **b-e**, Experimental STM images (tunneling parameters: b, V = 100 mV, I = 10 pA and c-e, V = -20 mV, I = 100 pA. See Supplementary Fig. S2 for substrate orientations). **f-i**, Experimental nc-AFM images obtained with a CO-functionalized tip (Δz = 275 pm, 165 pm, 210 pm, and, 195 pm for f-i the feedback loop was switched off with the parameters f: I = 40 pA, V = -5 mV; g: I = 100 pA, V = -5 mV; and, h-i: I = 100 pA, V = 5 mV, on the Au(111) surface). **j-m**, Simulated nc-AFM images (using the Probe-Particle model[31]) of the systems whose DFT-optimized geometry is represented in **n-q** (top views) and **r-u** (side views). Scale bars are 1 nm.

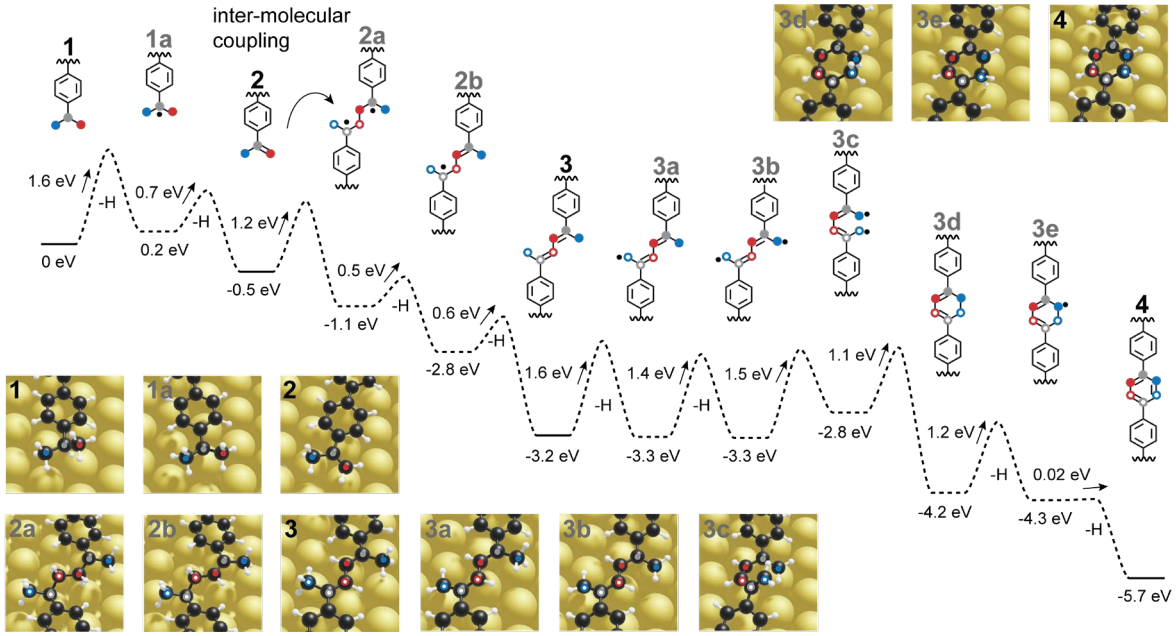

Fig. 4 | Theoretical investigation of the reaction mechanism. The energy barriers of all individual reaction steps are estimated by means of DFT optimizations along a specific reaction coordinates. The scheme of the reaction mechanism is represented with only the terminal phenylene ring and the three carbon atoms constituting the isopropyl group above the energy profile. The calculations are performed by starting from **1**. The DFT-computed energy barriers for each step are plotted in scale, after subtracting the energy of formation of **1** and the experimentally observed species are labelled in black while the intermediates are in grey. The calculations account for the entropic contribution from the desorption of the hydrogen molecules (-1 eV per H atom)[36]. The loss of hydrogen atoms is indicated by –H below the energy profile of the reaction step where C-H bonds are broken. Geometry optimized structures of **1** to **4** are shown labelled beside the energy profile. The carbon atoms participating in the cycloaromatization are labelled with red, grey, and blue for better comparison with the reaction pathway described in chemical structures.

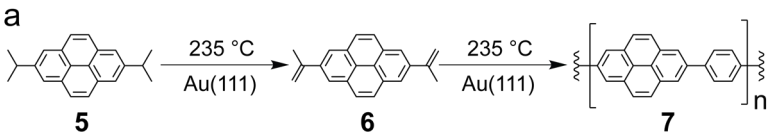

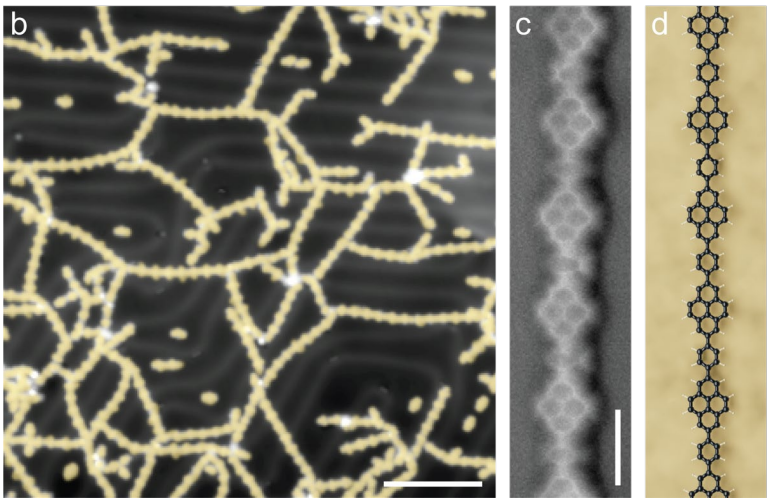

Fig. 5 | Formation of pyrenylene-phenylene copolymers. a, On-surface synthesis of the copolymer poly(2,7-pyrenylene-1,4-phenylene). **5** is synthesized in solution and deposited on an Au(111) surface held at 235°C, where it is thermally dehydrogenated toward **6** and subsequently polymerized to **7**. **b,** Overview STM image showing the resulting copolymers with alternating pyrene and phenylene moieties on the Au(111) surface (tunneling parameters: I = 100 pA, V = -1 V; scale bar: 10 nm). **c,** Bond-resolved nc-AFM image of a polymer chain showing the alternating pyrenylene and phenylene repeat units (Δz = 0 pm, feedback loop switched off at the set-point of: I = 120 pA, V = -10 mV in the center of the lowermost pyrene moiety scale bar: 1 nm). **d,** Sketch of the structure shown in **c**.

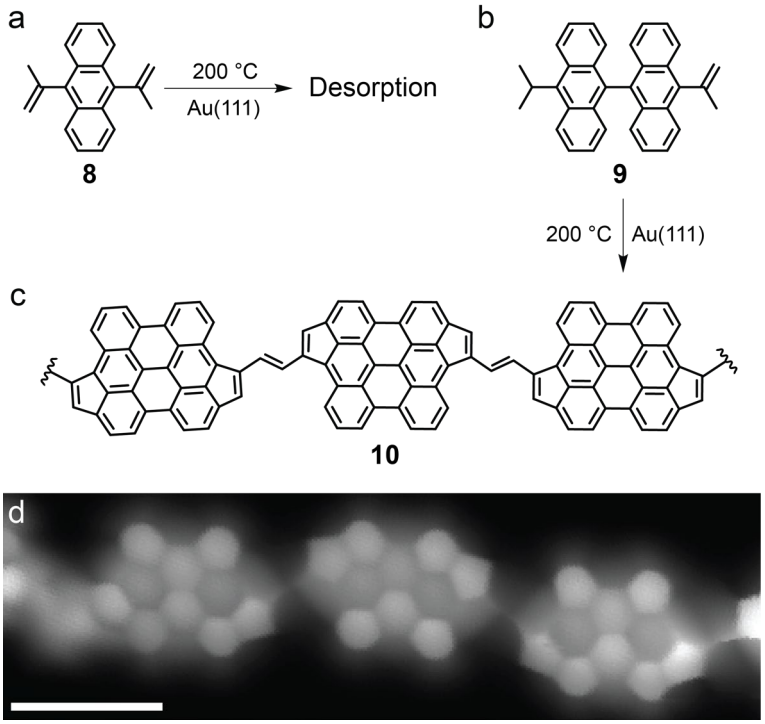

Fig. 6 | Design constraints on the [3+3] cycloaromatization reaction. a, 9,10-diisopropenylanthracene (**8**) desorbs from the surface before polymerization can occur. **b-c**, 10-isopropenyl-10'-isopropyl-9,9'-bianthracenyl (**9**), upon deposition and subsequent annealing on Au(111), forms oligomeric chains of **10**. **d,** Bond-resolved STM image of **10** revealing the mirror-symmetric formation of 5-membered rings, the chemical structure of the chain is shown in **c**. (Δz is -50 pm, feedback loop switched off at the set-point of I = 100 pA, V = -10 mV in the center of the leftmost perianthracenyl moiety. Scale bar is 1 nm).

References

1. Qiu, Z., Hammer, B. A. G. & Müllen, K. Conjugated polymers – Problems and promises. *Progress in Polymer Science* **100**, 101179 (2020).
2. Cheng, Y.-J., Yang, S.-H. & Hsu, C.-S. Synthesis of Conjugated Polymers for Organic Solar Cell Applications. *Chem. Rev.* **109**, 5868–5923 (2009).
3. Kawano, S. *et al.* Blue-Emitting Poly(2,7-pyrenylene)s: Synthesis and Optical Properties. *Macromolecules* **41**, 7933–7937 (2008).

4. Morin, P.-O., Bura, T. & Leclerc, M. Realizing the full potential of conjugated polymers: innovation in polymer synthesis. *Mater. Horiz.* **3**, 11–20 (2016).
5. Sakamoto, J., Rehahn, M., Wegner, G. & Schlüter, A. D. Suzuki Polycondensation: Polyarylenes à la Carte. *Macromolecular Rapid Communications* **30**, 653–687 (2009).
6. Yamamoto, T. Electrically conducting and thermally stable π-conjugated poly(arylene)s prepared by organometallic processes. *Progress in Polymer Science* **17**, 1153–1205 (1992).
7. Li, Y. *et al.* Energy Level and Molecular Structure Engineering of Conjugated Donor−Acceptor Copolymers for Photovoltaic Applications. *Macromolecules* **42**, 4491–4499 (2009).
8. Wu, P.-T., Kim, F. S., Champion, R. D. & Jenekhe, S. A. Conjugated Donor−Acceptor Copolymer Semiconductors. Synthesis, Optical Properties, Electrochemistry, and Field-Effect Carrier Mobility of Pyridopyrazine-Based Copolymers. *Macromolecules* **41**, 7021–7028 (2008).
9. Wu, J.-S., Cheng, S.-W., Cheng, Y.-J. & Hsu, C.-S. Donor–acceptor conjugated polymers based on multifused ladder-type arenes for organic solar cells. *Chem. Soc. Rev.* **44**, 1113–1154 (2015).
10. Müllen, K. & Pisula, W. Donor–Acceptor Polymers. *J. Am. Chem. Soc.* **137**, 9503–9505 (2015).
11. Suraru, S.-L., Lee, J. A. & Luscombe, C. K. C–H Arylation in the Synthesis of π-Conjugated Polymers. *ACS Macro Lett.* **5**, 724–729 (2016).
12. Pouliot, J.-R., Grenier, F., Blaskovits, J. T., Beaupré, S. & Leclerc, M. Direct (Hetero)arylation Polymerization: Simplicity for Conjugated Polymer Synthesis. *Chem. Rev.* **116**, 14225–14274 (2016).
13. Leclerc, M., Brassard, S. & Beaupré, S. Direct (hetero)arylation polymerization: toward defect-free conjugated polymers. *Polym J* **52**, 13–20 (2020).
14. Blaskovits, J. T. & Leclerc, M. C□H Activation as a Shortcut to Conjugated Polymer Synthesis. *Macromolecular Rapid Communications* **40**, 1800512 (2019).
15. Grill, L. *et al.* Nano-architectures by covalent assembly of molecular building blocks. *Nature Nanotech* **2**, 687–691 (2007).
16. Grill, L. & Hecht, S. Covalent on-surface polymerization. *Nat. Chem.* **12**, 115–130 (2020).
17. Clair, S. & de Oteyza, D. G. Controlling a Chemical Coupling Reaction on a Surface: Tools and Strategies for On-Surface Synthesis. *Chem. Rev.* **119**, 4717–4776 (2019).

18. Shen, Q., Gao, H.-Y. & Fuchs, H. Frontiers of on-surface synthesis: From principles to applications. *Nano Today* **13**, 77–96 (2017).

19. Hla, S.-W., Bartels, L., Meyer, G. & Rieder, K.-H. Inducing All Steps of a Chemical Reaction with the Scanning Tunneling Microscope Tip: Towards Single Molecule Engineering. *Phys. Rev. Lett.* **85**, 2777–2780 (2000).

20. Mistry, A. *et al.* The Synthesis and STM/AFM Imaging of 'Olympicene' Benzo[cd]pyrenes. *Chemistry – A European Journal* **21**, 2011–2018 (2015).

21. Pavlicek, N. *et al.* On-surface generation and imaging of arynes by atomic force microscopy. *Nature Chem.* **7**, 623–628 (2015).

22. Oteyza, D. G. de *et al.* Direct Imaging of Covalent Bond Structure in Single-Molecule Chemical Reactions. *Science* 1238187 (2013) doi:10.1126/science.1238187.

23. Schuler, B. *et al.* Reversible Bergman cyclization by atomic manipulation. *Nature Chemistry* **8**, 220–224 (2016).

24. Zhong, D. *et al.* Linear Alkane Polymerization on a Gold Surface. *Science* **334**, 213–216 (2011).

25. Volger, H. C. Oxidative dimerization of β-substituted α-olefins by palladium acetate. *Recueil des Travaux Chimiques des Pays-Bas* **86**, 677–686 (1967).

26. Chen, S. & Hu, A. Recent advances of the Bergman cyclization in polymer science. *Sci. China Chem.* **58**, 1710–1723 (2015).

27. Sun, Q. *et al.* On-Surface Formation of One-Dimensional Polyphenylene through Bergman Cyclization. *J. Am. Chem. Soc.* **135**, 8448–8451 (2013).

28. Merino-Díez, N. *et al.* Width-Dependent Band Gap in Armchair Graphene Nanoribbons Reveals Fermi Level Pinning on Au(111). *ACS Nano* **11**, 11661–11668 (2017).

29. Gross, L., Mohn, F., Moll, N., Liljeroth, P. & Meyer, G. The Chemical Structure of a Molecule Resolved by Atomic Force Microscopy. *Science* **325**, 1110–1114 (2009).

30. Gross, L. *et al.* Bond-Order Discrimination by Atomic Force Microscopy. *Science* **337**, 1326–1329 (2012).

31. Hapala, P. *et al.* Mapping the electrostatic force field of single molecules from high-resolution scanning probe images. *Nature Communications* **7**, 11560 (2016).

32. Björk, J., Stafström, S. & Hanke, F. Zipping Up: Cooperativity Drives the Synthesis of Graphene Nanoribbons. *J. Am. Chem. Soc.* **133**, 14884–14887 (2011).

33. Fan, Q. *et al.* Precise Monoselective Aromatic C–H Bond Activation by Chemisorption of *Meta* - Aryne on a Metal Surface. *Journal of the American Chemical Society* **140**, 7526–7532 (2018).

34. Floris, A. *et al.* Driving Forces for Covalent Assembly of Porphyrins by Selective C–H Bond Activation and Intermolecular Coupling on a Copper Surface. *J. Am. Chem. Soc.* **138**, 5837–5847 (2016).

35. Flory, P. J. The Mechanism of Vinyl Polymerizations [1]. *J. Am. Chem. Soc.* **59**, 241–253 (1937).

36. Bjork, J. Thermodynamics of an Electrocyclic Ring-Closure Reaction on Au (111). *The Journal of Physical Chemistry C* **120**, 21716–21721 (2016).

37. Pavliček, N. *et al.* Polyyne formation via skeletal rearrangement induced by atomic manipulation. *Nature Chemistry* (2018) doi:10.1038/s41557-018-0067-y.

38. Senkovskiy, B. V. *et al.* Making Graphene Nanoribbons Photoluminescent. *Nano Lett.* **17**, 4029–4037 (2017).

39. Borin Barin, G. *et al.* Optimized graphene transfer: Influence of polymethylmethacrylate (PMMA) layer concentration and baking time on graphene final performance. *Carbon* **84**, 82–90 (2015).

40. Xu, X. *et al.* On-Surface Synthesis of Dibenzohexacenohexacene and Dibenzopentaphenoheptaphene. *BCSJ* **94**, 997–999 (2021).

41. Weiss, C. *et al.* Imaging Pauli Repulsion in Scanning Tunneling Microscopy. *Phys. Rev. Lett.* **105**, 086103 (2010).

42. Kichin, G., Weiss, C., Wagner, C., Tautz, F. S. & Temirov, R. Single Molecule and Single Atom Sensors for Atomic Resolution Imaging of Chemically Complex Surfaces. *J. Am. Chem. Soc.* **133**, 16847–16851 (2011).

43. Fan, Q. *et al.* On-Surface Pseudo-High-Dilution Synthesis of Macrocycles: Principle and Mechanism. *ACS Nano* **11**, 5070–5079 (2017).

44. Giessibl, F. J. Atomic resolution on Si(111)-(7×7) by noncontact atomic force microscopy with a force sensor based on a quartz tuning fork. *Applied Physics Letters* **76**, 1470–1472 (2000).

45. Bartels, L. *et al.* Dynamics of Electron-Induced Manipulation of Individual CO Molecules on Cu(111). *Phys. Rev. Lett.* **80**, 2004–2007 (1998).

46. Yakutovich, A. V. *et al.* AiiDAlab – an ecosystem for developing, executing, and sharing scientific workflows. *Computational Materials Science* **188**, 110165 (2021).

47. Pizzi, G., Cepellotti, A., Sabatini, R., Marzari, N. & Kozinsky, B. AiiDA: automated interactive infrastructure and database for computational science. *Computational Materials Science* **111**, 218–230 (2016).

48. Hutter, J., Iannuzzi, M., Schiffmann, F. & VandeVondele, J. cp2k: atomistic simulations of condensed matter systems. *Wiley Interdisciplinary Reviews: Computational Molecular Science* **4**, 15–25 (2014).

49. VandeVondele, J. & Hutter, J. Gaussian basis sets for accurate calculations on molecular systems in gas and condensed phases. *The Journal of Chemical Physics* **127**, 114105 (2007).

50. Goedecker, S., Teter, M. & Hutter, J. Separable dual-space Gaussian pseudopotentials. *Phys. Rev. B* **54**, 1703–1710 (1996).

51. Perdew, J. P., Burke, K. & Ernzerhof, M. Generalized Gradient Approximation Made Simple. *Phys. Rev. Lett.* **77**, 3865–3868 (1996).

52. Grimme, S., Antony, J., Ehrlich, S. & Krieg, H. A consistent and accurate ab initio parametrization of density functional dispersion correction (DFT-D) for the 94 elements H-Pu. *J. Chem. Phys.* **132**, 154104 (2010).

53. Hanke, F. & Björk, J. Structure and local reactivity of the Au(111) surface reconstruction. *Phys. Rev. B* **87**, 235422 (2013).

54. Hapala, P. *et al.* Mechanism of high-resolution STM/AFM imaging with functionalized tips. *Phys. Rev. B* **90**, 085421 (2014).

55. Laio, A. & Parrinello, M. Escaping free-energy minima. *Proceedings of the National Academy of Sciences* **99**, 12562–12566 (2002).

56. Henkelman, G., Uberuaga, B. P. & Jónsson, H. A climbing image nudged elastic band method for finding saddle points and minimum energy paths. *The Journal of Chemical Physics* **113**, 9901–9904 (2000).

57. E, W., Ren, W. & Vanden-Eijnden, E. String method for the study of rare events. *Phys. Rev. B* **66**, 052301 (2002).

58. Kinikar, A. *et al.* On-Surface Polyarylene Synthesis by Cycloaromatization of Isopropyl Substituents. Materials Cloud Archive, doi: 10.24435/materialscloud:yy-sc. (2022).

59. Cai, Z., She, L., Wu, L. & Zhong, D. On-Surface Synthesis of Linear Polyphenyl Wires Guided by Surface Steric Effect. *J. Phys. Chem. C* **120**, 6619–6624 (2016).